Appendix A

Attenuation of Microwaves in Atmospheric Gases

Two atmospheric gases, oxygen and water vapor, contribute to attenuation of microwave radiation in clear atmosphere. Specific attenuation caused by oxygen A_{O_2} depends on the microwave frequency f, atmospheric pressure$P$, and temperature T (Ulaby et al. 1981):

$$A_{O_2} = 1.110^{-2} f^2 \frac{P}{1013}\left(\frac{300}{T}\right)^2 \gamma\left[\frac{1}{\left(f - f_{O_2}\right)^2 + \gamma^2} + \frac{1}{f^2 + \gamma^2}\right]. \tag{A.1}$$

In (A.1), $f_{O_2} = 60$ GHz,

$$\gamma = \gamma_0 \frac{P}{1013}\left(\frac{300}{T}\right)^{0.85} \quad \text{(GHz)},$$

$$\gamma_0 = \begin{cases} 0.59 & P > 333 \text{ mb} \\ 0.59[1 + 3.1 \times 10^{-3}(333 - P)] & 25 < P < 333 \text{ mb} \\ 1.18 & P < 25 \text{ mb} \end{cases}.$$

Specific attenuation caused by water vapor depends on the same parameters and absolute humidityρ_v:

$$A_{H_2O} = 2f^2 \rho_v \left(\frac{300}{T}\right)^{3/2} \gamma_1 \left[\left(\frac{300}{T}\right) e^{-644/T} \frac{1}{\left(f^2 - f_{H_2O}^2\right)^2} + 1.210^{-6}\right], \tag{A.2}$$

where $f_{H_2O} = 22.2$ GHz and

$\gamma_1 = 2.85 \frac{P}{1013}\left(\frac{300}{T}\right)^{0.626}\left(1 + 0.018 \frac{\rho_v T}{P}\right)$ (GHz).

A. V. Ryzhkov, D. S. Zrnic, *Radar Polarimetry for Weather Observations*,
Springer Atmospheric Sciences, https://doi.org/10.1007/978-3-030-05093-1

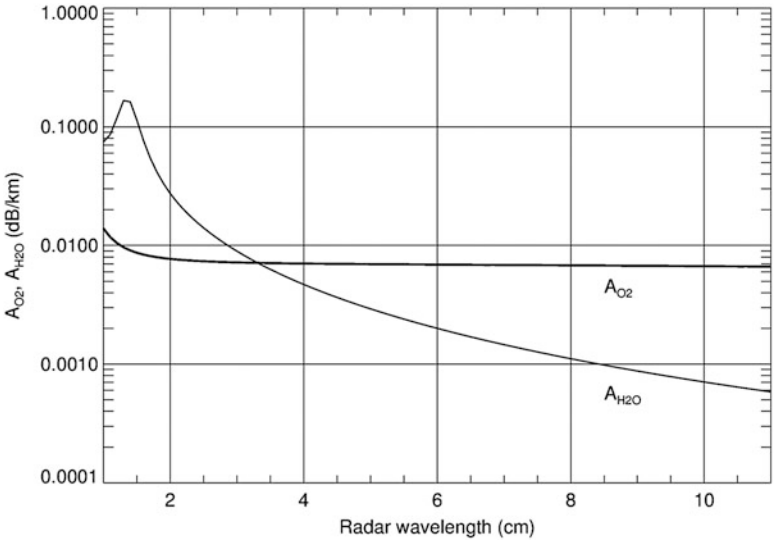

Fig. A.1 Wavelength dependencies of specific attenuations of the microwave radiation in oxygen and water vapor ($\rho_v = 7.5$ g m^{-3})

In (A.1) and (A.2), A_{O_2} and A_{H_2O} are expressed in dB km^{-1}, f is in GHz, P is in mb, T is in K°, and ρ_v is in g m^{-3}. Approximations (A.1) and (A.2) are valid for $f < 45$ GHz and $f < 100$ GHz.

Wavelength dependencies of A_{O_2} and A_{H_2O} are plotted in Fig. A.1 for $P = 1013$ mb, $T = 20$°C, and $\rho_v = 7.5$ g m^{-3}. It is evident that A_{H_2O} is a strong function of wavelength and reaches its maximum at $\lambda = 1.35$ cm corresponding to the water vapor absorption line, whereas A_{O_2} does not vary much for λ changing between 3 and 11 cm. The equations (A.1) and (A.2) indicate the dependence on temperature and pressure. These variables vary systematically with height above ground and cause predictable decrease in attenuation with increase in altitude.

Reference

Ulaby, F., Moore, R., & Fung, A. (1981). *Microwave remote sensing. Active and passive* (Vol. 1). Boston: Artech House. 456pp.

Appendix B

Angular Moments

Here we present analytical formulas for the angular moments defined by (3.45)

$$A_1 =< \sin^2\psi \cos^2\alpha >, \quad A_2 =< \sin^2\psi \sin^2\alpha >, \quad A_3 =< \sin^4\psi \cos^4\alpha >,$$
$$A_4 =< \sin^4\psi \sin^4\alpha >, \quad A_5 =< \sin^4\psi \cos^2\alpha \sin^2\alpha > \tag{B.1}$$

for the following three special cases.

Random Orientation of Hydrometeors

Assume that the scatterers are randomly oriented in the horizontal plane (i.e., azimuth angle ϕ is between 0 and 2π), the beam elevation is 0^o (a good approximation for surveillance radars), and the angle between axis of scatterer and horizontal plane is uniformly distributed from 0 to $\pi/2 - \theta_v$ (angle θ_v is measured with respect to the true vertical). The maximum deviation of $(\pi/2 - \theta_v)$ is referred as a "flutter angle" and this model is well suited for representing prolate shaped ice crystals like needles or chaff (Zrnic and Ryzhkov 2004; Melnikov and Straka 2013). The probability density function that represents a uniform distribution of orientation within these prescribed limits is

$$p(\theta, \phi) = \sin\theta/(2\pi \cos\theta_v). \tag{B.2}$$

The relations between the α, ψ, θ, and ϕ angles

A. V. Ryzhkov, D. S. Zrnic, *Radar Polarimetry for Weather Observations*,
Springer Atmospheric Sciences, https://doi.org/10.1007/978-3-030-05093-1

$$\begin{aligned} \sin\theta\cos\phi &= \sin\alpha\sin\psi \\ \cos\theta &= \sin\psi\cos\alpha \\ \cos\psi &= \sin\theta\sin\phi \end{aligned} \tag{B.3}$$

are needed to integrate various terms in (B.1). Two of the equations in (B.3) are independent, but three are listed for convenience (these are substituted into various integrands). Then integration with the prescribed distribution produces the following closed-form solutions for the angular moments $<A_i>$:

$$\begin{aligned} &A_1 = \cos^2\theta_v/3; \quad A_2 = \sin^2\theta_v/6 + 1/3; \quad A_3 = \cos^4\theta_v/5 \\ &A_4 = 3(\sin^4\theta_v - 4\cos^2\theta_v/3 + 4)/40; \quad A_5 = (\cos^2\theta_v/3 - \cos^4\theta_v/5)/2. \end{aligned} \tag{B.4}$$

For a fully random orientation $\theta_v = 0$ and (B.4) reduces to

$$A_1 = A_2 = 1/3; A_3 = A_4 = 1/5; A_5 = 1/15. \tag{B.5}$$

This result is independent of the elevation angle.

Random Orientation in the Horizontal Plane

This orientation is typical for columnar crystals; these tend to be oriented with their major dimensions in the horizontal plane.

$$A_1 = \frac{1}{2}\sin^2\beta, \quad A_2 = \frac{1}{2}, \quad A_3 = \frac{3}{8}\sin^4\beta, \quad A_4 = \frac{3}{8}, \quad A_5 = \frac{1}{8}\sin^2\beta \tag{B.6}$$

In (B.6), β is the elevation angle of the radar beam (Fig. 1.5).

Two-Dimensional Axisymmetric Gaussian Distribution of Orientation

This distribution can be approximated by (3.46) and it represents a wide class of atmospheric scatterers that can be modeled as oblate spheroids, including raindrops, snowflakes, graupel, and hail. The approximation (3.46) makes possible averaging over angles ψ and α independently, and the angular moments A_1—A_5 can be expressed as the products of the following factors:

$$
\begin{aligned}
&< \sin^2\psi >= \frac{1}{2}\left(1 - r_\sigma \cos 2\overline{\psi}\right),\\
&< \sin^4\psi >= \frac{3}{8} - \frac{1}{2} r_\sigma \cos 2\overline{\psi} + \frac{1}{8} r_\sigma^4 \cos 4\overline{\psi},\\
&< \cos^2\alpha >= \frac{1}{2}\left(1 + r_{\sigma\alpha} \cos 2\overline{\alpha}\right),\\
&< \sin^2\alpha >= \frac{1}{2}\left(1 - r_{\sigma\alpha} \cos 2\overline{\alpha}\right),\\
&< \cos^4\alpha >= \frac{3}{8} + \frac{1}{2} r_{\sigma\alpha} \cos 2\overline{\alpha} + \frac{1}{8} r_{\sigma\alpha}^4 \cos 4\overline{\alpha},\\
&< \sin^4\alpha >= \frac{3}{8} - \frac{1}{2} r_{\sigma\alpha} \cos 2\overline{\alpha} + \frac{1}{8} r_{\sigma\alpha}^4 \cos 4\overline{\alpha},\\
&< \cos^2\alpha \sin^2\alpha >= \frac{1}{8}\left(1 - r_{\sigma\alpha}^4 \cos 4\overline{\alpha}\right)
\end{aligned}
\tag{B.7}
$$

where

$$
r_\sigma = \exp\left(-2\sigma^2\right), \quad r_{\sigma\alpha} = \exp\left(-2\sigma_\alpha^2\right) \tag{B.8}
$$

If the mean canting angle is zero (a reasonable assumption for a majority of hydrometeors (Ryzhkov et al. 2002)), then at low antenna elevation angle $\overline{\psi} \approx \pi/2$ and the angular moments A_1—A_5 can be approximated by (Ryzhkov 2001)

$$
\begin{aligned}
&A_1 = \frac{1}{4}(1 + r_\sigma)^2, \quad A_2 = \frac{1}{4}\left(1 - r_\sigma^2\right), \quad A_3 = \left(\frac{3}{8} + \frac{1}{2} r_\sigma + \frac{1}{8} r_\sigma^4\right)^2,\\
&A_4 = \left(\frac{3}{8} - \frac{1}{2} r_\sigma + \frac{1}{8} r_\sigma^4\right)\left(\frac{3}{8} + \frac{1}{2} r_\sigma + \frac{1}{8} r_\sigma^4\right), \quad A_5 = \frac{1}{8}\left(1 - r_\sigma^4\right)\left(\frac{3}{8} + \frac{1}{2} r_\sigma + \frac{1}{8} r_\sigma^4\right)
\end{aligned}
\tag{B.9}
$$

References

Melnikov, V., & Straka, J. (2013). Axis ratios and flutter angles of cloud ice particles: Retrievals from radar data. *Journal of Atmospheric and Oceanic Technology, 30*, 1691–1703.

Ryzhkov, A. (2001). Interpretation of polarimetric radar covariance matrix for meteorological scatterers: Theoretical analysis. *Journal of Atmospheric and Oceanic Technology, 18*, 315–328.

Ryzhkov, A., Zrnic, D., Hubbert, J., Bringi, V., Vivekanandan, J., & Brandes, E. (2002). Polarimetric radar observations and interpretation of co-cross-polar correlation coefficients. *Journal of Atmospheric and Oceanic Technology, 19*, 340–354.

Zrnic, D., & Ryzhkov, A. (2004). Polarimetric properties of chaff. *Journal of Atmospheric and Oceanic Technology, 21*, 1017–1024.

Appendix C

Dielectric Constants of Water and Solid Ice

Formulas for the dielectric constants of water and solid ice as functions of temperature and wavelength are summarized here. The real and imaginary parts of ε for water and ice can be expressed as (Ray 1972)

$$\mathrm{Re}(\varepsilon) = \varepsilon_\infty + \frac{(\varepsilon_0 - \varepsilon_\infty)\left[1 + (\lambda_0/\lambda)^{1-\alpha}\sin(\alpha\pi/2)\right]}{1 + 2(\lambda_0/\lambda)^{1-\alpha}\sin(\alpha\pi/2) + (\lambda_0/\lambda)^{2(1-\alpha)}}, \tag{C.1}$$

$$\mathrm{Im}(\varepsilon) = \pm\left(\frac{(\varepsilon_0 - \varepsilon_\infty)(\lambda_0/\lambda)^{1-\alpha}\cos(\alpha\pi/2)}{1 + 2(\lambda_0/\lambda)^{1-\alpha}\sin(\alpha\pi/2) + (\lambda_0/\lambda)^{2(1-\alpha)}} + \frac{\sigma\lambda}{18.8496 \times 10^{10}}\right), \tag{C.2}$$

where in the case of water

$$\begin{aligned}
\varepsilon_0 &= 78.54[1.0 - 4.579 \times 10^{-3}(T - 25.0) + 1.19 \times 10^{-5}(T - 25)^2 \\
&\qquad -2.8 \times 10^{-8}(T - 25)^3] \\
\varepsilon_\infty &= 5.27137 + 0.021647\ T - 0.00131198\ T^2 \\
\alpha &= -16.8129/(T + 273) + 0.0609265 \\
\lambda_0 &= 0.00033836 \exp[2513.98/(T + 273)] \\
\sigma &= 12.5664 \times 10^8
\end{aligned} \tag{C.3}$$

and in the case of ice

A. V. Ryzhkov, D. S. Zrnic, *Radar Polarimetry for Weather Observations*,
Springer Atmospheric Sciences, https://doi.org/10.1007/978-3-030-05093-1

$$\begin{aligned}
\varepsilon_0 &= 203.168 + 2.5\ T + 0.15\ T^2 \\
\varepsilon_\infty &= 3.168 \\
\alpha &= 0.288 + 0.0052\ T + 0.00023\ T^2 \\
\lambda_0 &= 0.0009990288\ \exp\{13200/[(T + 273)\ 1.9869]\} \\
\sigma &= 1.26\ \exp\{-12500/[(T + 273)\ 1.9869]\}.
\end{aligned} \tag{C.4}$$

In Formulas (C.1)–(C.4), λ is the wavelength expressed in cm and T is the temperature in °C. Positive sign in Eq. (C.2) should be selected if the $\exp(-j\omega t)$ convention is assumed, and negative sign is appropriate in the case of the $\exp(j\omega t)$ convention.

Reference

Ray, P. (1972). Broadband complex refractive indices of ice and water. *Applied Optics, 11*, 1836–1844.

Appendix D

The Impact of Different Microphysical Factors on the Cross-Correlation Coefficient

To clarify how physical properties of atmospheric particles affect ρ_{hv}, let's consider a simple model with two scatterers, so that

$$
\begin{aligned}
\mid \rho_{hv} \mid e^{j\bar{\delta}} &= \frac{s_{hh}^{(1)*} s_{vv}^{(1)} + s_{hh}^{(2)*} s_{vv}^{(2)}}{\left(\left|s_{hh}^{(1)}\right|^2 + \left|s_{hh}^{(2)}\right|^2\right)^{1/2} \left(\left|s_{vv}^{(1)}\right|^2 + \left|s_{vv}^{(2)}\right|^2\right)^{1/2}} \\
&= \frac{\mid s_{hh}^{(1)} \mid\mid s_{vv}^{(1)} \mid e^{j\delta_1} + \mid s_{hh}^{(2)} \mid\mid s_{vv}^{(2)} \mid e^{j\delta_2}}{\left(\left|s_{hh}^{(1)}\right|^2 + \left|s_{hh}^{(2)}\right|^2\right)^{1/2} \left(\left|s_{vv}^{(1)}\right|^2 + \left|s_{vv}^{(2)}\right|^2\right)^{1/2}},
\end{aligned}
\tag{D.1}
$$

where superscripts 1 and 2 denote two different scatterers and δ_1 and δ_2 are their backscatter differential phases defined in (3.38). If $\delta_1 = \delta_2 = 0$ (which is a valid assumption for smaller size raindrops (Fig. 5.17)) then ρ_{hv} is a real number and

$$
\rho_{hv} = \frac{\mid s_{hh}^{(1)} \mid\mid s_{vv}^{(1)} \mid + \mid s_{hh}^{(2)} \mid\mid s_{vv}^{(2)} \mid}{\left(\left|s_{hh}^{(1)}\right|^2 + \left|s_{hh}^{(2)}\right|^2\right)^{1/2} \left(\left|s_{vv}^{(1)}\right|^2 + \left|s_{vv}^{(2)}\right|^2\right)^{1/2}}. \tag{D.2}
$$

Next consider several special cases to illustrate the impact of different microphysical factors on ρ_{hv}.

(a) Particles are spherical and have different sizes (Fig. D.1a), so that

A. V. Ryzhkov, D. S. Zrnic, *Radar Polarimetry for Weather Observations*,
Springer Atmospheric Sciences, https://doi.org/10.1007/978-3-030-05093-1

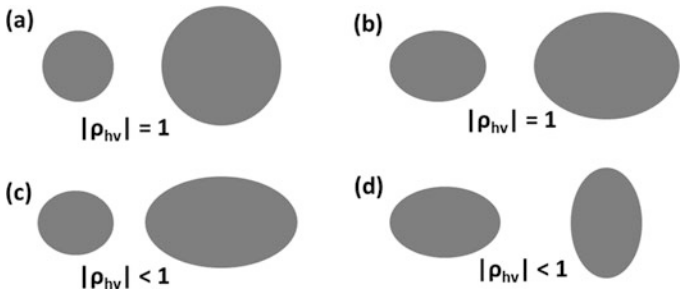

Fig. D.1 Magnitudes of the cross-correlation coefficient for different combinations of two particles in the radar resolution volume. (**a**) Spherical particles, (**b**) Nonspherical particles with equal axis ratios, (**c**) Nonspherical particles with different axis ratios, (**d**) Identical particles with different orientations

$$| s_{hh}^{(1)} | = | s_{vv}^{(1)} | = s_1, \quad | s_{hh}^{(2)} | = | s_{vv}^{(2)} | = s_2. \tag{D.3}$$

Then it follows from (D.2) that $\rho_{hv} = 1$ for arbitrary number of spherical particles of various sizes.

(b) Particles are nonspherical, have different sizes, similar shape, and same orientation (Fig. D.1b), so that

$$| s_{hh}^{(1)} | = p \, | s_{vv}^{(1)} | , \quad | s_{hh}^{(2)} | = p \, | s_{vv}^{(2)} | , \quad | s_{vv}^{(1)} | \neq | s_{vv}^{(2)} | . \tag{D.4}$$

Again, $\rho_{hv} = 1$. This means that if the axis ratio (which determines the parameter p) and canting angle do not change across the particle size distributions, then the magnitude of the cross-correlation coefficient is identically one. Note that the symmetry axis of both scatterers is vertically oriented in this example. Nonetheless, the result is invariant to the orientation as long as both (all) scatterers have the same orientation.

(c) Particles are nonspherical and have different sizes and same orientation, and their axis ratio changes as a function of size which is typical for rain because larger raindrops are more oblate than smaller ones (Fig. D.1c). Therefore

$$| s_{hh}^{(1)} | = p_1 \, | s_{vv}^{(1)} | , \quad | s_{hh}^{(2)} | = p_2 \, | s_{vv}^{(2)} | , \quad | s_{vv}^{(1)} | \neq | s_{vv}^{(2)} | , \quad p_1 \neq p_2, \tag{D.5}$$

and $\rho_{hv} < 1$. This leads to the important conclusion that variability of particle shapes across particle size spectra causes reduction of ρ_{hv}.

(d) Particles are nonspherical and have same size but different orientation. As an example, one scatterer has its rotation axis directed vertically and the other horizontally (Fig. D.1d). In this case,

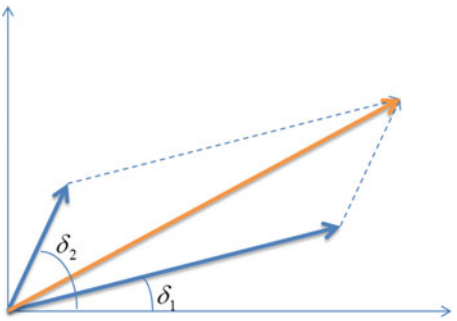

Fig. D.2 The impact of the difference between backscatter differential phases of two particles δ_2-δ_1 on the magnitude of the cross-correlation coefficient which is proportional to the length of the sum (orange) vector

$$| s_{hh}^{(1)} | = p \, | s_{vv}^{(1)} | , \quad | s_{hh}^{(2)} | = \frac{1}{p} | s_{vv}^{(2)} | , \quad | s_{vv}^{(1)} | = | s_{hh}^{(2)} | , \tag{D.6}$$

and it can be shown that $\rho_{hv} < 1$. Hence, variability of orientation of particles (identical or not identical) causes the drop in the cross-correlation coefficient.

(e) Two particles of the same size, shape, and orientation but with different phase composition (e.g., raindrop and dry/wet graupel, or two melting graupel particles with different fractional mass water contents).

The situation with such two particles is described by conditions (D.4) and (D.5) because neither their reflectivities nor differential reflectivities (i.e., ${p_1}^2$ and ${p_2}^2$) are equal. Therefore, $\rho_{hv} < 1$. Larger difference in the effective dielectric constants of the two hydrometeors lowers more their ρ_{hv}.

So far we assumed that $\delta_1 = \delta_2 = 0$. If $\delta_1 \neq \delta_2$, then ρ_{hv} depends on the difference between δ_1 and δ_2 because two terms in the numerator of (D.1) are summed up as vectors (Fig. D.2). The value of ρ_{hv} can be substantially reduced with increase in $|\delta_1 - \delta_2|$. Therefore, if the backscatter differential phase changes significantly across the particle size spectrum, ρ_{hv} tends to decrease. This happens, for example, in rain at C band if raindrop size distribution contains drops with sizes between 5 and 7 mm for which δ changes from $-15°$ to $45°$ (Fig. 5.17). The cross-correlation coefficient also decreases if hydrometeors with small intrinsic δ (such as raindrops) are mixed with hydrometeors having large δ (such as wet snowflakes or hailstones).

Index

A. V. Ryzhkov, D. S. Zrnic, *Radar Polarimetry for Weather Observations*,
Springer Atmospheric Sciences, https://doi.org/10.1007/978-3-030-05093-1